We are IntechOpen,
the world's leading publisher of
Open Access books
Built by scientists, for scientists

6,900
Open access books available

186,000
International authors and editors

200M
Downloads

Our authors are among the

154
Countries delivered to

TOP 1%
most cited scientists

12.2%
Contributors from top 500 universities

CLARIVATE ANALYTICS
BOOK CITATION INDEX
INDEXED

WEB OF SCIENCE™

Selection of our books indexed in the Book Citation Index
in Web of Science™ Core Collection (BKCI)

Interested in publishing with us?
Contact book.department@intechopen.com

RFID Localization in Wireless Sensor Networks

Yang Zhao and Neal Patwari

Additional information is available at the end of the chapter

Abstract

Received signal strength (RSS)-based localization of people and assets through RFID has significant benefits for logistics, security and safety. However, the accuracy of RFID localization in wireless sensor networks suffers from unrealistic antenna gain pattern assumption, and the human body has a major effect on the gain pattern of the RFID badge that the person is wearing. In this book chapter, the gain pattern due to the effect of the human body is experimentally measured and modeled. A method is presented to estimate the model parameters from multiple RSS measurements. Two joint orientation and position estimators, four-dimensional (4D) maximum likelihood estimation (MLE) algorithm and alternating gain and position estimation (AGAPE) algorithm, are proposed to estimate the orientation and the position of the badge using RSS measurements from anchor nodes. A Bayesian lower bound on the mean squared error of the joint estimation is derived and compared with the Cramer-Rao bound with an isotropic gain pattern. Both theoretical and experimental results show that the accuracy of position estimates can be improved with orientation estimates included in the localization system.

Keywords: localization, radio propagation, wireless sensor network

1. Introduction

RFID localization of assets, robots and people has significant benefits for logistics, security and operations management. For example, GE Healthcare uses the AgileTrac platform [1] to track the physical location of each asset, via various real-time location system (RTLS) techniques. In RFID localization, many kinds of radio measurements can be used: time of arrival (TOA), time difference of arrival (TDOA), angle of arrival (AOA) and received signal strength (RSS) [2]. While RSS is low-cost and available in almost all standard wireless devices, most RSS-based localization methods make the assumption that the transmitters have isotropic gain patterns. However, even when the antenna of a transmitter badge is considered as isotropic, people or objects can affect the RFID badge's radiation, due to the fact that they are absorbing power, altering the antenna impedance and thus distorting the antenna gain pattern [3]. Previous

studies have focused on characterizing the effects of a human body's location and orientation on RSS measurements [4–7]. In this book chapter, we present models and methods to handle, and in fact benefit from, the removal of the unrealistic isotropic gain pattern assumption.

Real-world directional gain patterns are problematic for RSS-based localization algorithms. In RSS-based algorithms, a model relating RSS and path length is assumed [8] or estimated from training measurements [9]. When the RFID antenna gain pattern is no longer isotropic, the distances estimated from the log-distance model [10] will not be the same even if the RFID transmitter is in the middle of two receivers. Model-based localization algorithms will infer that the transmitter is closer to the receiver that measured larger RSS and will thus produce estimates that are biased towards directions of high gain in the gain pattern [3].

To deal with the non-isotropic antenna gain pattern and improve model-based RFID localization algorithm, we need to build a model for the directionality of a transmitter RFID badge when it is worn by a person or attached to an object. We present measurements and models for a transmitter badge worn by a person. However, RFID tags attached to large objects will also experience non-isotropic gain patterns, and thus extensions to other types of tagged objects are feasible. As presented in the study of Zhao et al. [3], the variation of RSS was modeled as a function of people's orientation (i.e., facing direction). The study also proposed (1) a first-order model to capture most of the variation in the gain pattern as a function of people's orientation, (2) a method to estimate people's orientation and directionality from ordinary RSS measurements, and (3) an algorithm to estimate the position, orientation and gain pattern of the RFID badge called alternating gain and position estimation (AGAPE) algorithm. We apply the AGAPE algorithm together with a 2D maximum likelihood estimation (MLE) algorithm [8] and 4D MLE algorithm [3] to three sets of experiments performed at different environments: outdoor, indoor and through-wall. Experimental results show different levels of improvement from including the first-order gain pattern model at those different environments.

It is not obvious that a non-isotropic gain pattern can benefit RFID localization because additional model parameters must be estimated together with the RFID locations. In addition to experimental results, we provide theoretical results that show that the existence of a directional gain pattern can actually reduce position error for localization algorithms. The Bayesian Cramer-Rao bound (Bayesian CRB) was derived in Ref. [3] for joint estimation of orientation and position, while the CRB for position estimation was derived in Ref. [8] with an isotropic gain pattern assumption. Comparison between the Bayesian CRB [3] and the CRB [8] shows that joint estimation of orientation and position may outperform (result in lower mean squared error) estimation of position alone in the isotropic case.

In summary, in this book chapter, we present the latest research progress in the effort to include RFID antenna gain pattern in model-based RSS localization algorithms. We show that real-world non-isotropic gain pattern of RFID badge is not a problem to be ignored, but a means to improve localization accuracy. We present measurements, models, estimation algorithms and estimation lower bounds for RSS-based localization in wireless sensor networks. Experimental results from three sets of experiments show that position estimates are improved with the inclusion of orientation estimates from the first-order gain pattern model and the RSS measurements.

2. Models

Statistical models based on real-world measurements are important for model-based RSS localization algorithms. In this section, a measurement-based model is presented for the gain pattern of a transmitter badge worn by a person. A transmitter in close proximity to a human body is strongly affected by human tissue, which absorbs power and distorts the gain pattern of the transmitter [11, 12].

The log-distance model [10] is a general model for the power P_i received at anchor node i *from the transmitter badge t*. We include the transmitter gain pattern in the log-distance model, and the dBm power P_i is modeled as

$$P_i = P_0 - 10n_p \log_{10}\left(\frac{d_i}{d_0}\right) + g(\alpha_i) + \eta \tag{1}$$

where P_0 is the received power in dBm at a reference distance d_0, n_p is the pathloss exponent, d_i is the distance between anchor node i and transmitter badge t, α_i is the angle between anchor node i and the badge, $g(\alpha_i)$ is the gain pattern of the transmitter badge at angle α_i, and η is the model error plus noise. Note that the log-distance model parameters P_0 and n_p can be estimated using the received RSS measurements between pairs of anchor nodes. Assuming known anchor node coordinates, these two model parameters can be estimated via linear regression, as in Ref. [8].

Naive model-based localization algorithms use $g(\alpha_i) = 0$ for all α_i. We propose to include a nonzero $g(\alpha_i)$ in Eq. (1). Any real-world gain pattern will depend on the person and the badge and will look somewhat random; however, we hope to capture the major features of $g(\alpha_i)$ that will be largely accurate for the average person.

2.1. Measurements

The recent study in Ref. [3] quantifies the effect of the orientation of a human body on the RSS measurements using datasets from several experiment campaigns. In their experimental study, two Crossbow TelosB nodes [13] operating at 2.4 GHz were used with one node (node 1) placed on a stand and the other one (node 2) hung in the middle of a person's chest. The person wearing node 2 turned 45° every 20 s, with the distance between these two nodes kept the same. Meanwhile, the RSS at node 1 was recorded on a computer. Node 2 transmitted about 20 times per second, thus about 400 RSS measurements were recorded for each of the eight different orientations made by the person. The described experiments were performed by five people in the student building as well as an empty parking lot at University of Utah. Eight experiments were performed with various distances between the two nodes from 1.5 to 5.0 m. Therefore, a total of 25,600 measurements were recorded.

Experimental results from two different experiments are shown in **Figure 1(a)**. The minimum RSS of Experiment 1 (red) and Experiment 2 (blue) are 145° and 180°, respectively, whereas the maximum RSS are 315°and 0°, respectively. **Figure 1(b)** shows the mean gain pattern, which is averaged across all experiments, and indicates that if the person's orientation is 180°, i.e., the human body blocks the line-of-sight (LOS) path between nodes 1 and 2, the gain pattern is close
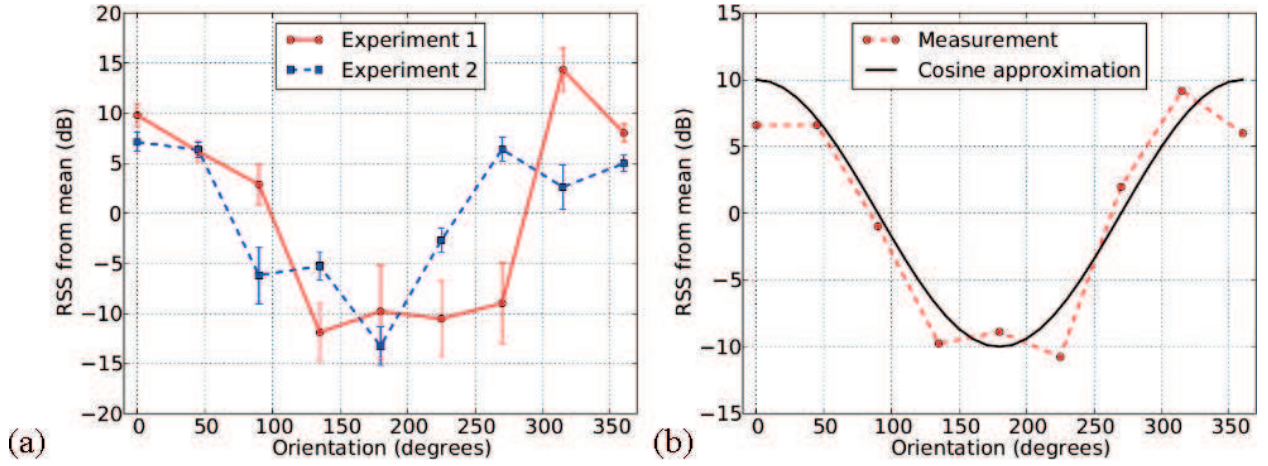
Figure 1. The effect of the human body on the RFID antenna gain pattern (RSS from mean). (a) Measured gain patterns with the error bars in two different experiments. (b) Average over all measured data.

to the minimum. In contrast, if the person's orientation is 0°, i.e., facing the node1, then the gain pattern is about 20 dB higher as compared with its lowest point [the red curve in **Figure 1(b)**]. The average gain pattern in **Figure 1(b)** closely resembles a cosine function (black curve) with period 360° and amplitude 10 dB. It is worth to note that the variation in RSS as a function of orientation due to the presence of a person is similar to other experimental studies [7, 14].

2.2. Gain pattern model

Based on the results of the measurements described above, a model for the gain pattern is proposed as a cosine function with period 360°:

$$\hat{g}(\alpha) = G_1 \cos(\alpha - \beta) \qquad (2)$$

where β is the orientation (direction of maximum gain) of the badge, and $G_1 \geq 0$ is the magnitude of the cosine function in dB, which we also refer to as the directionality, and $G_1 = 0$ indicates no directionality, i.e., the RFID badge is an isotropic radiator.

As explained in Ref. [3], the model of Eq. (2) represents the two most important characteristics observed in the measurements. First, regardless of path length or person wearing the badge, the gain is higher in the direction the person is facing and lower in the opposite direction. In a wireless sensor network with several anchor nodes, a person with a badge stands halfway between node j and node k so that the distance between the badge and these two nodes are the same, as shown in **Figure 2**. Given that the person is facing node k, the mean RSS value of node k would be greater than that of node j.

Second, Eq. (2) is a first-order model for any periodic function. The measurements for this particular set of data showed a single order captures the vast majority of the angular variation. Any function with period 2π has a Fourier series representation as the follows:

$$g(\alpha) = \frac{1}{2\pi} \sum_{k=-\infty}^{\infty} G(k) e^{j2\pi k\alpha} \qquad (3)$$
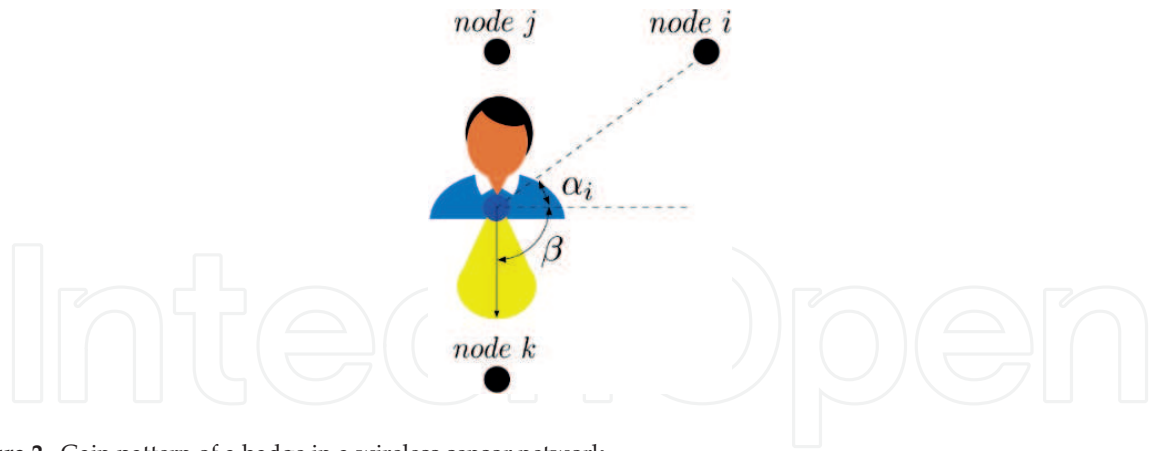
Figure 2. Gain pattern of a badge in a wireless sensor network.

where $G(k)$ are the complex-valued Fourier series components. Note that the model of Eq. (2) is simply the first harmonic of an arbitrary gain pattern measurement. That is, we include only the $k = 1$ term in Eq. (3).

3. Localization algorithms

3.1. Problem statement

This chapter focuses on 2D position estimation using RSS measurements. For a wireless sensor network which has N anchor nodes and one badge, the position estimation corresponds to the estimation of the coordinates of a badge: $z_t = [x_t, \; y_t]^T$. Note that one badge is used to simplify notation in the chapter. However, extension to multiple badges is possible.

If we only use the log-distance model in Ref. [10] to estimate distances between the badge and anchor nodes, our unknown model parameter $\theta = z_t$, since the other model parameters n_p and P_0 can be determined using pairwise RSS measurements between N anchor nodes.

However, if the gain pattern model is included, two parameters in the gain pattern model must be estimated from Eq. (2). So, we include these two parameters as nuisance parameters, and the unknown parameter vector θ becomes:

$$\boldsymbol{\theta} = [z_t^T, \beta, G_1]^T \tag{4}$$

where β is the orientation of the RFID badge, and G_1 is the directionality of the RFID antenna gain pattern.

3.2. 4D MLE algorithm

To estimate both the badge position and the gain pattern, a baseline algorithm - 4D maximum likelihood estimation (MLE) algorithm is introduced here as the counterpart of the 2D MLE algorithm [8] with an isotropic antenna gain pattern assumption.

As discussed in Section 2, the received dBm power P_i is modeled as Eq. (1). Assuming the RSS values P_i are independent Gaussian with variance σ^2 and mean $\mu(\theta) = P_0 - 10n_p\log_{10}\left(\frac{d_i}{d_0}\right) + g(\alpha_i)$, one can show that the MLE of the badge position is as follows:

$$\hat{\boldsymbol{\theta}}_{MLE} = \underset{\theta}{\text{argmax}} \sum_{i=0}^{N-1} \left(P_i - \mu(\boldsymbol{\theta})\right)^2 \tag{5}$$

As mentioned in Ref. [3], grid search method was used for finding the MLE solution. For instance, in the isotropic gain pattern case, the TICC2431 used a 2D grid search method to find the 2D coordinate. However, when the dimension of the estimation parameter vector increases, the computation time of a grid search increases exponentially. In addition, the high computation cost of a multi-dimensional gird search also prevents it from real-time applications. To better estimate the position and the gain pattern in real-time, we use signal processing techniques and first-order approximation to develop a different algorithm.

3.3. Gain pattern estimator

Before we propose the algorithm to jointly estimate the position and the gain pattern, we first introduce a gain pattern estimator, assuming we know the badge position z_t. The gain pattern estimator was first proposed in Ref. [3], and we present their work in this section.

When measuring the gain pattern at discrete values of α_i, $i = 0, 1 \cdots N - 1$, we require the discrete Fourier transform (DFT) instead of the Fourier series. However, the same principle applies—the cosine with period 2π is the first-order approximation of the gain function. Specifically, for the gain pattern at angle α_i, the discrete-time exponential representation is given by

$$g(\alpha_i) = \frac{1}{N}\sum_{k=0}^{N-1} G(k)e^{j\alpha_i k} = \frac{1}{N}G(0) + \frac{2}{N}\sum_{k=1}^{M} |G(k)| \cos\left(\angle G(k) + \alpha_i k\right) \tag{6}$$

where $M = \frac{N}{2}$, and $\alpha_i = \frac{2\pi i}{N}$, for N equally spaced measurements. In the measurement experiments, we had $N = 8$.

The mean gain $G(0)$ is simply the average of all of the differences (which we call the model error) between P_i and the log-distance path loss model, that is, $P_0 - 10n_p\log_{10}\left(\frac{d_i}{d_0}\right)$. Because n_p and P_0 are determined by linear regression, they tend to make the model error zero mean. Thus, we assume that $G(0) = 0$ dB because any mean model error would have been removed by the linear regression.

Then, the gain pattern from an M order model can be estimated as:

$$\hat{g}_{M(\alpha_i)} = \frac{2}{N}\sum_{k=1}^{M} |G(k)| \cos\left(\angle G(k) + \alpha_i k\right) \tag{7}$$

The first-order model including only the $k = 1$ term in (7) is

$$\hat{g}(\alpha_i) = \frac{2}{N}|G(1)|\cos(\angle G(1) + \alpha_i) \tag{8}$$

By comparing Eqs. (8) and (2) in Section 2.2, we find the two model parameters β and G_1 of the gain pattern can be calculated as:

$$\beta = -\angle G(1)$$

$$G_1 = \frac{2}{N}|G(1)| \tag{9}$$

Thus to estimate the gain pattern, we only need to calculate the DFT term $G(1)$. In the measurement experiments discussed in Section 2.1, it was possible to measure the gain at equally spaced angles. In real deployments, anchor nodes will make measurements at a variety of non-equally spaced angles α_i, depending on badge and anchor node positions. The most common way to estimate the spectral content in a signal using non-equally spaced samples is simply to apply the DFT to the available samples [15]. Thus, we estimate $G(k)$ as:

$$G(k) = \sum_{i=0}^{N-1} g(\alpha_i)e^{-j\alpha_i k} \tag{10}$$

where $g(\alpha_i)$ can be calculated from Eq. (1), knowing the received power and the angle between the badge and anchor nodes.

Note, we need only $G(1)$ for the first-order model of Eq. (2). This calculation of $G(1)$ requires only N complex multiplies and adds, where N is the number of RSS measurements received for a badge. This low complexity is important to minimize the computational complexity of the localization algorithm.

3.4. Alternating gain and position estimator

In the gain pattern estimation, the badge position is assumed known. But in a localization algorithm, the badge position needs to be estimated. For joint position and gain pattern estimation, an alternating gain and position estimation (AGAPE) algorithm has been developed in Ref. [3] to efficiently estimate both the position and orientation of a person in a wireless sensor network.

As described in Ref. [3], the algorithm includes (1) the initial estimation of the position of the badge using isotropic gain assumption, (2) calculation of the gain pattern parameters using the first-order sinusoidal model, (3) re-estimation of the badge position using the RSS-distance model with the estimated gain pattern. The algorithm iterates until a misfit function is minimized. Note that the proposed AGAPE algorithm is a kind of alternating minimization method [16]. **Figure 3** shows the flowchart of the AGAPE algorithm. For the first step, given that the gain pattern is isotropic, the naive MLE method is used to estimate the badge position. The MLE solution can be derived from a conjugate gradient algorithm. However, a 2D grid
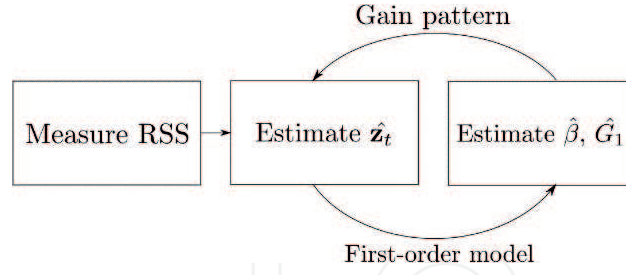
Figure 3. Flowchart of the AGAPE algorithm.

search method was used to avoid the local minima problem here, in the position estimation step. Note that the 2D MLE grid search can be accomplished quickly in hardware. The output of the position estimation step is referred to as $\hat{z}_t$.

For the orientation estimation step, given an estimated position, we calculate the gain pattern $g(\alpha_i)$ from the RSS-distance model Eq. (1), and then, the DFT term $G(1)$ is calculated from Eq. (10). The gain pattern model parameters orientation β and directionality G_1 are then estimated from $\angle G(1)$ the phase angle of $G(1)$ and the magnitude of $G(1)$, respectively, as given in Eq. (9). Finally, the position of the badge is estimated using the RSS-distance model with estimated orientation and directionality again. The steps of position and orientation estimation repeat until the following misfit function is minimized:

$$\mathbf{\Phi} = \sum_{i=1}^{N} (P_i - \widehat{P}_i)^2 \tag{11}$$

where $\widehat{P}_i$ is the RSS estimate at anchor node i, which is calculated from the RSS-distance model Eq. (1).

4. Estimator lower bounds

One might think that the lower bound of the variance of an estimator will increase due to the introduction of an additional unknown gain pattern model. In this section, the Bayesian CRB [17] is derived by including the gain pattern model parameters as nuisance parameters, as derived in Ref. [3]. The Bayesian CRB is used because the prior knowledge of the gain directionality G_1 is available a priori. In this book chapter, we show that the CRB derived in Ref. [8] is a special case of the Bayesian CRB derived here. We also show that the lower bound on the variance of a position estimator is decreased by the introduction of a gain pattern model.

4.1. Bayesian CRB

To derive the Bayesian CRB, we assume that the orientation of the badge β is uniformly distributed in the range of 0–2π because the orientation of the person wearing the badge is arbitrary.

The gain pattern model expressed in Eq. (2) can be rewritten as:

$$g(\alpha_i) = G_I \cos \alpha_i + G_Q \sin \alpha_i \tag{12}$$

where $G_I = G_1 \cos \beta$, $G_Q = G_1 \sin \beta$. Here, we assume the in-phase component G_I and quadrature component of G_Q are i.i.d. Gaussian distributed with zero means and variance σ_G^2. Components G_I and G_Q are affected by many different factors, such as the person's shape and size, and also the badge location on the human body. Thus, their distributions are close to Gaussian, by a central limit argument. This assumption is equivalent to a Rayleigh distribution [18] assumption for G_1, which matches the prior knowledge of G_1: (1) G_1 must have a nonnegative value; (2) G_1 is unlikely to be exactly zero and also unlikely to have very large values, since the gain pattern is related to human size.

The Bayesian CRB is also called the Van Trees bound or the MSE bound [17], it is given by:

$$\mathrm{var}(\boldsymbol{\theta}) \geq (I_D + I_P)^{-1} \tag{13}$$

where $\theta = [z_t^T, G_I, G_Q]^T$, I_D represents the Fisher information matrix, and I_P represents the prior information matrix [17]. Note that the prior information only contains information of the gain pattern, no prior information about the badge position is included. The detailed derivation of the Bayesian CRB is presented in Ref. [3], we compare it with the CRB derived with an isotropic gain pattern assumption next.

4.2. Comparison with CRB

For an estimator with deterministic parameters, a CRB is often used. With an isotropic gain pattern assumption, a CRB for position estimation using RSS is derived in Ref. [8]. When the gain pattern term in the RSS-distance model approaches zero, that is, $g(\alpha_i) = 0$, the Bayesian CRB should be the same as the CRB derived in Ref. [8]. We show this next.

With the additional parameters in the gain pattern model, the Bayesian CRB not only depends on radio channel parameters, but also depends on gain pattern parameter σ_G^2. Once
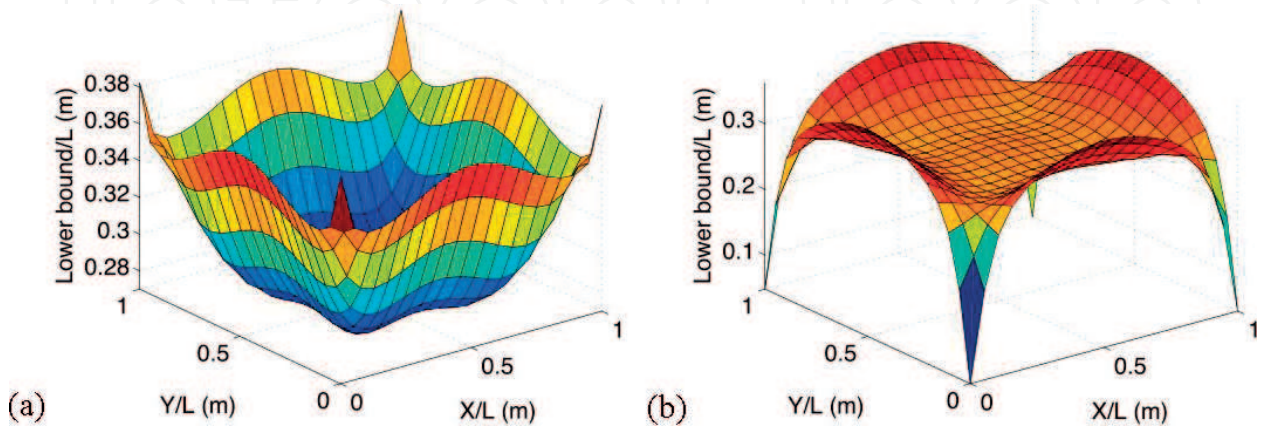

Figure 4. Lower bounds. (a) Lower bound with $\sigma_G^2 = 0.0001$ (minimum value: 0.27, maximum value: 0.38). (b) Lower bound with $\sigma_G^2 = 1$ (minimum value: 0.05, maximum value: 0.36).

these model parameters are calculated, the Bayesian CRB can be calculated for an L m by L m square area with four anchor nodes located at four corners. If we use the same radio channel parameters as [8] and two different σ_G^2 values: $\sigma_G^2 = 0.0001$ and $\sigma_G^2 = 1$, the two Bayesian CRBs are shown in **Figure 4**. For very small σ_G^2, *e.g.*, $\sigma_G^2 = 0.0001$, the Bayesian CRB is shown in **Figure 4(a)**, which is identical to the CRB derived in Ref. [8]. For $\sigma_G^2 = 1$, the Bayesian CRB is shown in **Figure 4(b)**. To obtain a lower bound for the overall area, we introduce the *average RMSE bound*, which is defined as the average value of the square root of the Bayesian CRB bounds over the area. The average RMSE bound for $\sigma_G^2 = 1$ is 0.29 m, which is lower than the 0.30 m average RMSE bound with a gain pattern close to isotropic, *e.g.*, $\sigma_G^2 = 0.0001$.

5. Experiments and results

5.1. Experiment description

We present experimental datasets from three experiment campaigns in this book chapter. These experiments were performed at outdoor, indoor and through-wall scenarios, which cover a variety of multipath effects and environmental noise conditions.

- *Experiment 1*: The first experiment was performed in a 6.4 m by 6.4 m area outside the Merrill Engineering Building of the University of Utah. The area is surrounded by 28 TelosB nodes [13] deployed at known locations on stands at 1 m height, near trees and 3 m away from the building wall. A person worn a TelosB node in the middle of his chest and walked around a marked path at a constant speed of about 0.5 m/s. This outdoor experiment dataset was first reported in Ref. [3], and details can be found there.

- *Experiment 2*: The second experiment was an indoor experiment performed inside the Warnock Engineering Building of the University of Utah. A 6.1 m by 6.1 m area was surrounded by 20 TelosB nodes with an interdistance of 0.91 m between each two anchor nodes. A person wearing a TelosB node walked clockwise twice around a 2.7 m by 2.7 m square, as shown as the purple line in **Figure 9**. The experiment was performed in the building lounge area, during which students occasionally walked outside the peripheral area of the sensor network. This experiment is first reported in this book chapter.

- *Experiment 3*: The third experiment was a through-wall experiment, in which 34 TelosB nodes were deployed outside the living room of a residential house, as shown in **Figure 5 (b)**. A person wearing a transmitter walked four times around a 3.6 m by 3.6 m square in the living room. The experiment was performed in a dynamic environment, where wind caused tree branches and leaves to sway. This experiment dataset is first reported in Ref. [19].

5.2. Experiment test bed and procedure

All three experiments use the same radio hardware, network protocol and follow the same procedure. TelosB nodes were used as network anchor nodes and also mobile node. In all
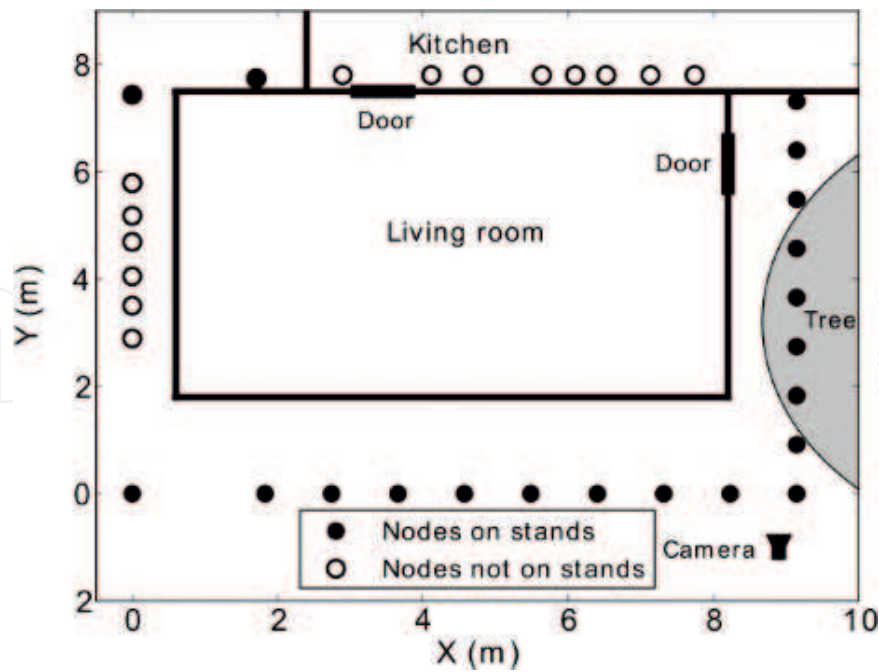
Figure 5. Experiment layout of Experiment 3 (through-wall).

experiments, anchor nodes were deployed at fixed locations, and one mobile node (transmitter badge) was worn by a person in the middle of their chest. All TelosB nodes were programmed with TinyOS program Spin [21] SPAN Lab. Spin protocol, and a base station connected to a laptop was used to collect RSS measurements received by all the anchor nodes.

Before people started walking in the area, a calibration was performed with no people in the experimental area. Since the locations of the anchor nodes are known, we use the measured RSS and the link length to estimate the n_p and P_0 parameters of the log-distance model. During the experiment, a person wearing the radio transmitter on their chest walked around a marked path a few times. A metronome and a metered path were used to keep the walking speed constant so that the position of the person at any particular time was known. The actual positions and orientations of the badge during these experiments are both known, so we can compare them with the position and orientation estimates from the AGAPE algorithm.

5.3. Experimental results

A unique feature of modeling RFID antenna gain pattern is that it enables estimating the orientation of the person, in addition to the person's location. We show the orientation estimation results from the AGAPE algorithm using data from Experiment 1, which was first reported in Ref. [3]. The estimated orientations are shown in **Figure 6**, together with the actual walking directions. The orientation estimates generally agree well with the actual orientations. As mentioned in Ref. [3], "the deviations from the actual orientations are generally less than 30°. However, sometimes when the person is turning, the bias is larger than 30°. This may be due to the fact that the algorithm uses RSS measurements from 28 anchor nodes to estimate the person's orientations, and at the turning points, RSS measurements may be a mix of those
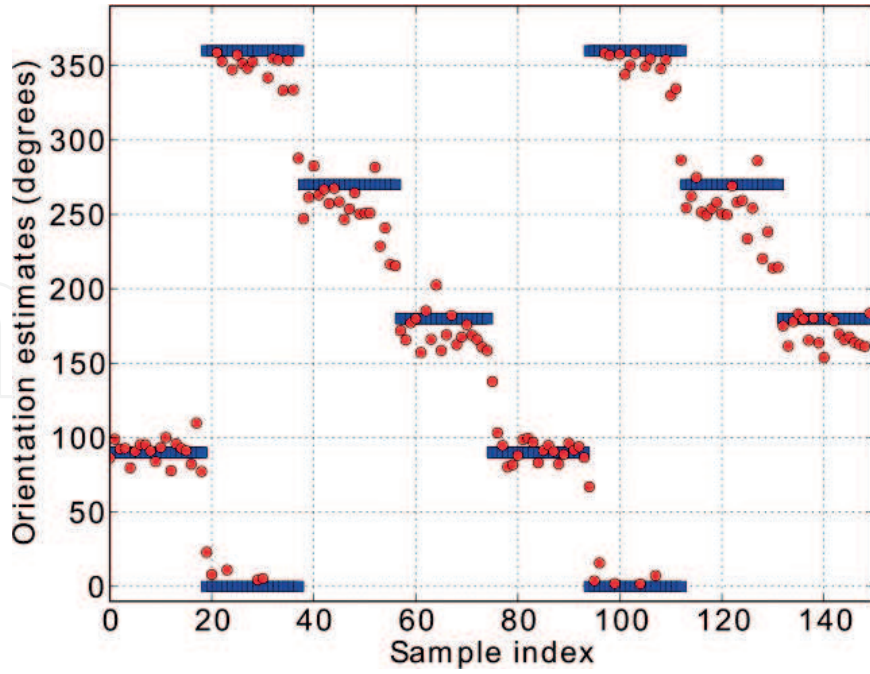
Figure 6. Mobile's actual orientations (■) and orientation estimates (○) (time for each sample is about 0.4 s).

recorded before, after and during turning." The median error from the AGAPE algorithm is about 10°, and more than 90% errors are below 30°. The 4D MLE algorithm can also estimate orientation, but it takes much more computing time. As mentioned in Ref. [3], the 4D MLE implementation uses "10 times more than the AGAPE algorithm in the Python implementation, and the estimates are not more accurate than those from AGAPE." In addition to the orientation of the badge, another model parameter G_1 is also estimated. For Experiment 1, G_1 has an averaged value of 12, which suggests that "the directionality of the gain of the transmitter badge worn by this particular person in this particular environment is about 12 dB."This value is consistent with our experiments in the antenna gain pattern modeling discussed in Section 2.

For the performance of position estimation, the CDF of the position estimation error from Experiment 1 is shown in **Figure 7**. We see that the median estimation error is about 0.61 m, and the 90th percentile estimation error is 1.22 m. However, the 2D MLE method has a median error of 2.60 m, which is about 4.3 times larger than that from AGAPE. From the comparison of the CDFs, we see that significant improvement is made if we include the orientation estimate in the localization.

In Experiment 1, a wireless sensor network with 28 anchor nodes is used to locate a badge in a 6.4 m by 6.4 m square area. However, not so many anchor nodes may be available in some applications. The following tests are performed using RSS measurements from a fraction of all anchor nodes to investigate the effect of node number on the localization accuracy.

As mentioned in Ref. [3], "in the first test—Test 1, we use RSS measurements from different numbers of equally spaced anchor nodes to locate the badge. For example, we first choose the RSS measurements from four anchor nodes at each corner of the square area. As expected, the
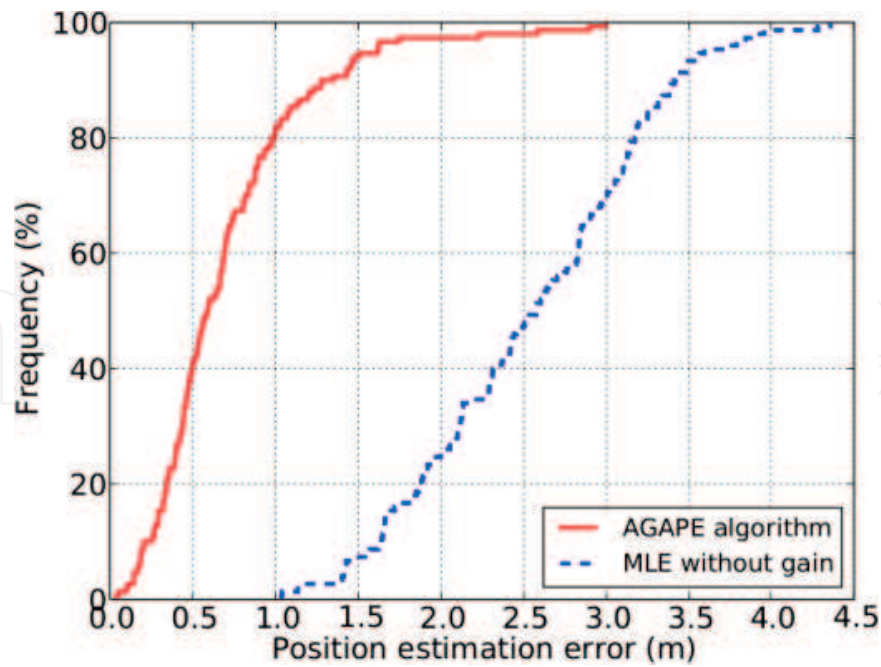
Figure 7. CDFs of position estimation errors from AGAPE and 2D MLE.

localization is not very accurate, the RMSE of the position estimate is 3.36 m, and the RMSE of the orientation estimate is 40°. Next, we use the RSS measurements from those anchor nodes whose ID numbers are multiples of 1, 2, 3 and 4 (since the anchor nodes are placed in a numerically increasing order around the experimental area, these anchor nodes are equally spaced). The RMSEs of the position and orientation estimates are shown as dots in **Figure 8(a)** and **(b)**, respectively. We see that as the node number increases, the RMSEs of position and orientation estimates both decrease. When the node number increases to fourteen, the RMSE of the position estimate decreases to 1.30 m, and the RMSE of the orientation estimate decreases to 18°. Further increase in anchor nodes will continue to decrease the RMSEs, however, there are diminishing returns."
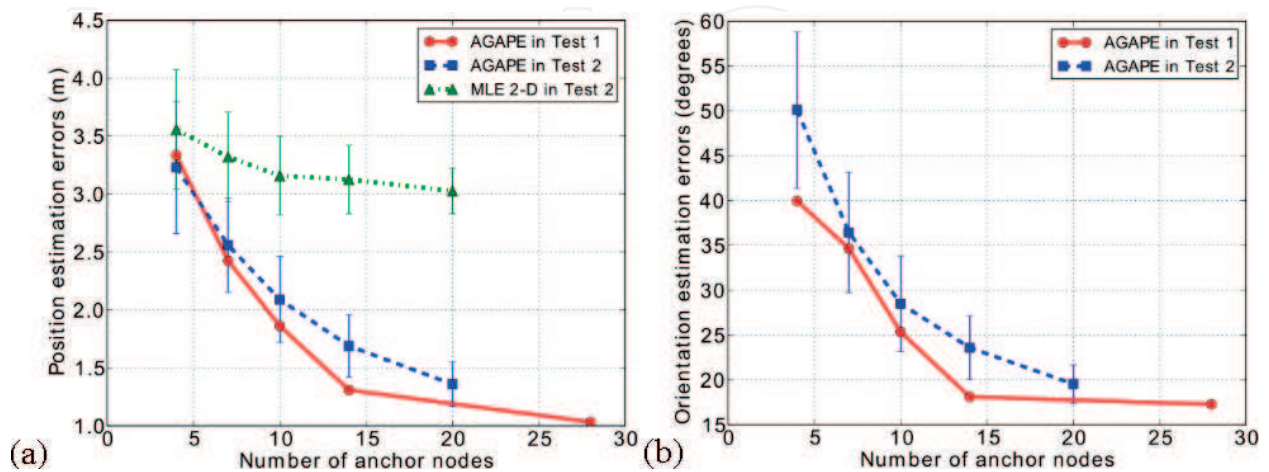

Figure 8. Effect of node number on (a) position estimation error and (b) orientation estimation error. (Test 1 uses equally spaced anchor nodes and Test 2 uses randomly chosen anchor nodes).

"In practical scenarios, anchor nodes may not be equally spaced. Thus, in Test 2, we use RSS measurements from randomly chosen anchor nodes. For example, we randomly choose four anchor nodes and run AGAPE using the RSS measurements from these nodes. We repeat the above procedure 100 times, and each time calculate the RMSEs of the position and orientation estimates. Similarly, we randomly choose seven, ten, fourteen and twenty anchor nodes. The average RMSEs are shown as squares, and the RMSE standard deviations are shown as error bars in **Figure 8**. From **Figure 8(b)**, we see that the average orientation RMSEs in Test 2 are all larger than the RMSEs in Test 1. For position RMSEs shown in **Figure 8(a)**, the average RMSEs in Test 2 are generally larger than the RMSEs in Test 1, except for the extreme case when the number of anchor nodes is four. Thus, the AGAPE algorithm generally performs better if the anchor nodes are equally spaced. However, the AGAPE algorithm is not very sensitive to the effect of anchor nodes being non-equally spaced. In fact, the differences between the position RMSEs in Test 1 and the average position RMSEs in Test 2 are always less than 0.4 m. Finally, we compare the performance of the naive MLE 2D method with the AGAPE algorithm using randomly chosen nodes. As shown in **Figure 8(a)**, the MLE 2D method is not very sensitive to the number of anchor nodes. However, the average position RMSEs from the MLE 2D method are always larger than those from the AGAPE algorithm for different numbers of anchor nodes."

For Experiment 1, we see that the AGAPE algorithm can estimate both the orientation and location of a person wearing an RFID badge with good accuracy for an outdoor environment. However, its performance degrades at the indoor and through-wall experiments, i.e., in Experiments 2 and 3. The position estimates from AGAPE and 2D MLE at a particular time in Experiment 2 are shown in **Figure 9**, together with the likelihood function of MLE. We see the MLE location estimate is biased towards the walking direction of the person, as it does not include the human body effect on the transmitter gain pattern in its model. We also see that the AGAPE algorithm is able to estimate both position and orientation of the person, and the position estimate is closer to the actual location than the 2D MLE estimate. However, AGAPE is not as accurate as in the outdoor experiments, because the modeling error in the first-order gain pattern model increases at an indoor environment due to multipath effects.

For the through-wall experiment Experiment 3, we see that due to the attenuation of walls, the path-loss model parameter $n_p = 3.22$, which is much larger than those from the first two experiments. The AGAPE algorithm can still estimate both the position and orientation of the person with reasonable accuracy, but there are several position estimate errors that are larger than 4 m (not shown in the figure). This is due to the ambiguity problem of AGAPE since AGAPE has orientation β and gain pattern parameter G_1 to estimate, in addition to position estimate. That is, AGAPE can converge to an incorrect position with an incorrect estimate of orientation due to the noisy RSS measurements and the modeling error.

We compare the root mean squared error (RMSE) of the position estimates for the above three sets of experiments. The RMSEs from the AGAPE, 2D MLE and 4D MLE algorithms are listed in **Table 1**. We see that for Experiment 1, the RMSE from the AGAPE algorithm is 0.87 m, which is similar to the 4D MLE algorithm. However, the MLE 4D algorithm uses grid search method and is not a real-time algorithm due to its computational complexity. The RMSE from
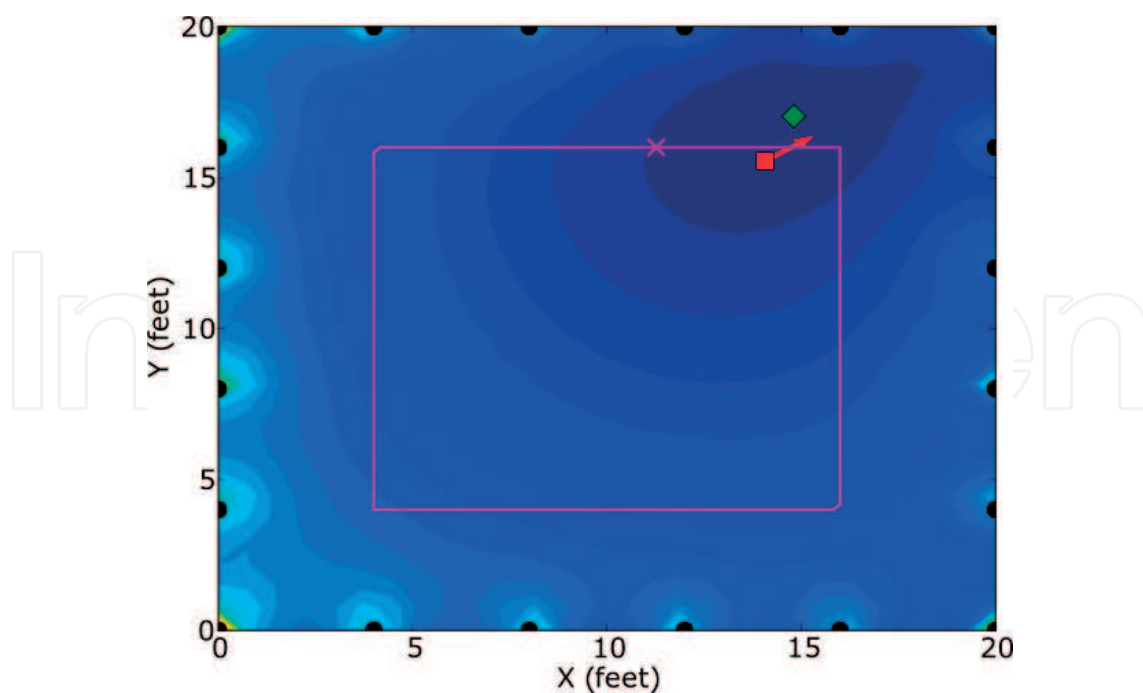
Figure 9. MLE likelihood and position estimates from 2D MLE and AGAPE algorithms in Experiment 2. Marked walking path (purple line); actual person position (×); 2D MLE position estimate (◊); AGAPE position estimate (▪) and AGAPE orientation estimate (→).

Experiment	Model parameters		RMSE from MLE (2D) in meter	RMSE from MLE (4D) in meter	RMSE from AGAPE in meter
	n_p	P_0			
Experiment 1	1.67	48.6	2.64	0.98	1.03
Experiment 2	2.28	19.8	1.86	1.65	1.69
Experiment 3	3.22	30.5	2.10	2.02	2.05

Table 1. Experimental localization results: RMSEs from MLE (2D), MLE (4D) and AGAPE.

the 2D MLE algorithm is 2.64 m. So for Experiment 1, the RMSE from AGAPE is reduced by 67.2% compared to the 2D MLE algorithm. For Experiment 2, the 2D MLE has an RMSE of 1.86 m, while the RMSEs from 4D MLE and the AGAPE are 1.65 and 1.69 m, with 11% and 9% improvement, respectively. Finally, for Experiment 3, AGAPE does not have much improvement compared to MLE. Both MLE and AGAPE have RMSEs of about 2 m.

From the above comparison, we see that the 4D MLE and AGAPE algorithms are significantly more accurate than the 2D MLE algorithm for outdoor environments. The 4D MLE takes much more time than the AGAPE algorithm, but both algorithms can estimate the position and orientation of a person wearing an RFID badge in front of her chest. The benefit from the modeled directional gain pattern reduces at indoor and through-wall environments, since the first-order gain pattern model becomes much noisier due to the increased multipath effects.

The AGAPE and 4D MLE algorithms may suffer from the ambiguity problem, that is, they may converge to a wrong position with a wrong orientation estimate. This ambiguity problem is observed when a person wearing an RFID badge presents in close proximity to walls. This problem may be resolved using orientation estimates from inertial measurement unit (IMU). However, RF device-free localization [19, 20] may provide a simple way to solve the ambiguity issue without adding more sensing modalities.

6. Conclusion

In this book chapter, we present measurements and models of active RFID antenna gain pattern due to the human body effect. We find that a wireless sensor network-based RFID localization system can actually benefit from the non-isotropic gain pattern due to the attenuation and reflection of the human body. We present three estimation methods of RFID localization using received signal strength (RSS) measurements from a wireless sensor network: 2D maximum likelihood estimator (MLE), 4D maximum likelihood estimator (MLE) and alternating gain and position estimator (AGAPE). The 4D MLE and AGAPE algorithms can both estimate user orientation in addition to position, with the first-order gain pattern model and the assumption that the user is wearing the RFID badge in front of her chest. However, the AGAPE algorithm significantly outperforms the 4D MLE algorithm in computational time using discrete Fourier transform (DFT) and first-order approximation. We also derive theoretical estimation lower bound for joint orientation and position estimation problem. The Bayesian Cramer-Rao bound (CRB) shows that the lower bound on the variance of a position estimator decreases with the inclusion of a gain pattern model to the RSS log-distance model. Finally, we present three sets of experiments performed at outdoor, indoor and through-wall environments. The experimental results show that the 4D MLE and AGAPE algorithms outperform the 2D MLE algorithm in localization accuracy in all datasets.

Author details

Yang Zhao[1]* and Neal Patwari[2]

*Address all correspondence to: yang.zhao@ge.com

1 General Electric Global Research Center, Niskayuna, NY, USA

2 Department of Electrical and Computer Engineering, University of Utah, Salt Lake City, UT, USA

References

[1] GE Healthcare. AgileTrac [Internet]. 2012. Available from: http://www3.gehealthcare.com.au/en-au/solutions/hom/agiletrac

[2]   G. Mao, B. Fidan, and B.D.O. Anderson. Wireless sensor network localization techniques. Computer Networks. 2007;**51**:2529-2553

[3]   Y. Zhao, N. Patwari, P. Agrawal, and M. Rabbat. Directed by directionality: benefiting from the gain pattern of active RFID badges. IEEE Transactions on Mobile Computing. 2012;**11**:865-877

[4]   P. Bahl, and V.N. Padmanabhan. RADAR: an in-building RF-based user location and tracking system. In: IEEE Infocom; 2000. p. 775-784

[5]   A.M. Ladd, K. Bekris, G. Marceau, A. Rudys, L. Kavraki, and D. Wallach. Robotics-based location sensing using wireless ethernet. In: Conference on Mobile Computing and Networking (MobiCom); 2002. p. 227-238

[6]   A. Howard, S. Siddiqi, and G. Sukhatme. An experimental study of localization using wireless ethernet. In: The International Conference on Field and Service Robotics; 2003. p. 201-206

[7]   K. Kaemarungsi, and P. Krishnamurthy. Properties of indoor received signal strength for WLAN location fingerprinting. In: The 1st Annual International Conference on Mobile and Ubiquitous Systems: Networking and Services (MobiQuitous); 2004. p. 14-23

[8]   N. Patwari, A.O. Hero III, M. Perkins, N. Correal, and R.J. O'Dea. Relative location estimation in wireless sensor networks. IEEE Transactions on Signal Processing. 2003;**51**: 2137-2148

[9]   T. Roos, P. Myllymki, H. Tirri, P. Misikangas, and J. Sievnen. A probabilistic approach to WLAN user location estimation. International Journal of Wireless Information Networks. 2002;**9**:155-164

[10] T.S. Rappaport. Wireless communications: principles and practice. NJ: Prentice-Hall Inc.; 1996

[11] M. Jensen, and Y. Rahmat-Samii. EM interaction of handset antennas and a human in personal communications. Proceedings of the IEEE. 1995;**83**:7-17

[12] J. Griffin and G. Durgin. Complete link budgets for backscatter radio and RFID systems. IEEE Antennas and Propagation Magazine. 2009;**51**:11-25

[13] Wiki. TelosB [Internet]. 2010. Available from: http://tinyos.stanford.edu/tinyos-wiki/index. php/TelosB

[14] T. King, S. Kopf, T. Haenselmann, C. Lubberger, and W. Effelsberg. COMPASS: A probabilistic indoor positioning system based on 802.11 and digital compasses. In: Proceedings of the 1st International Workshop on Wireless Network Testbeds, Experimental Evaluation and Characterization; 2006. p. 34-40

[15] N. Lomb. Least-squares frequency analysis of unequally spaced data. Astrophysics and space science. 1976;447-462

[16] A. Gunawardana and W. Byrne. Convergence theorems for generalized alternating minimization procedures. Journal of Machine Learning Research. 2005;**6**:2049-2073

[17] H.L. Van Trees. Detection, Estimation, and Modulation Theory, Part I. John Wiley & Sons; New York, Chichester; 1968

[18] S. Miller, and D. Childers. Probability and random processes: with applications to signal processing and communications. Academic Press; 2004

[19] Y. Zhao, and N. Patwari. Robust estimators for variance-based device-free localization and tracking. IEEE Transactions on Mobile Computing. 2015;**14**:2116-2129

[20] J. Wilson, and N. Patwari. Radio tomographic imaging with wireless networks. IEEE Transactions on Mobile Computing. 2010;**9**:621-632

[21] SPAN Lab. Spin protocol [Internet]. Available from: http://span.ece.utah.edu/spin